

Dynamics and Mechanism of Intercalation/De-Intercalation of Rhodamine B during the Polymorphic Transformation of the CdAl Layered Double Hydroxide to the Brucite-like Cadmium Hydroxide

Daniel Saliba,[†] Alaa Ezzeddine,[‡] Abdul-Hamid Emwas,[§] Niveen M. Khashab,[‡] and Mazen Al-Ghoul^{*,†}

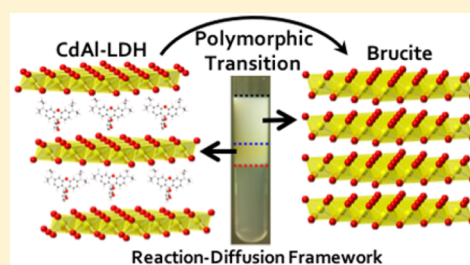
[†]Department of Chemistry, American University of Beirut, P.O. Box 11-0236, Riad El-Solh 1107 2020, Beirut, Lebanon

[‡]Smart Hybrid Materials (SHMs) Lab, King Abdullah University of Science and Technology (KAUST), Thuwal 23955-6900, Kingdom of Saudi Arabia

[§]Imaging and Characterization Core Lab, King Abdullah University of Science and Technology (KAUST), Thuwal, Kingdom of Saudi Arabia

Supporting Information

ABSTRACT: We studied the kinetics of intercalation of a fluorescent probe (rhodamine B (RhB)) during the formation of hierarchal microspheres of cadmium–aluminum layered double hydroxide (CdAl LDH) and its de-intercalation upon transformation from the LDH phase into the cadmium hydroxide β phase ($\text{Cd}(\text{OH})_2$) using a reaction-diffusion framework (RDF) where the hydroxide anions diffuse into an agar gel matrix containing the proper salts–fluorescent probe mixture. In this framework, we achieved the stabilization of the CdAl LDH, which is known to be thermodynamically unstable and transforms into $\text{Cd}(\text{OH})_2$ and $\text{Al}(\text{OH})_3$ in a short period. RDF is advantageous as it allows with ease the extraction of the cosynthesized polymorphs and their characterization using X-ray diffraction (XRD), differential scanning calorimetry (DSC), thermal gravimetric analysis (TGA), solid-state nuclear magnetic resonance (SSNMR), Fourier transform infrared (FT-IR), and energy dispersive X-ray (EDX). The kinetics of inter/de-intercalation is studied using *in situ* steady-state fluorescence measurements. The existence of RhB in the LDH layers and its expel during the transition into the β phase are examined via fluorescence microscopy, XRD, and SSNMR. The activation energies of intercalation and de-intercalation of RhB are determined and show dependence on the cationic ratio of the corresponding LDH. We find that the energies of de-intercalation are systematically higher than those of intercalation, indicating that the dyes are stabilized due to the probe–brucite sheets interactions. SSNMR is used to shed light on the mechanism of intercalation and stabilization of RhB inside the layers of the LDH.



INTRODUCTION

Layered double hydroxides (LDHs), also termed hydrotalcite-like compounds, are anionic clays endowed with a wide variety of applications in various scientific processes (catalysts precursors, catalysts, etc.).^{1–3} The structure of these LDHs is better understood starting from that of the brucite compounds, $\text{M}(\text{II})(\text{OH})_2$, where the divalent metal cations ($\text{M}(\text{II})$) are octahedrally surrounded by hydroxyl groups which share edges to form infinite neutral sheets.⁴ The stacking of these sheets on top of each other forms a tridimensional structure, the brucite compounds. The random substitution of some of the divalent cations by trivalent ones generates an excess in the positive charges in the sheets.^{1,5} It results in the intercalation of some charge-balancing anions accompanied by water and/or other neutral molecules in the interlayer region to reestablish the electroneutrality of the compound, thus forming anionic LDHs. In addition to the intercalation of small anions (such as chlorides and nitrates), larger anions, including biomolecules and polyelectrolytes, can also intercalate. For example, graphene oxide nanosheets were intercalated into a calcium/aluminum LDH rendering the material amenable to many

interesting and diverse functions including electronic applications,⁶ arsenate removal from water,⁷ and biosensing.⁸ Generally, the chemical formula of anionic LDHs is $[\text{M}(\text{II})_{1-x}\text{M}(\text{III})_x(\text{OH})_2]^{x+}(\text{A}^{n-})_{x/n} \cdot m\text{H}_2\text{O}$, namely, $\text{M}(\text{II})\text{M}(\text{III})\text{-A}$, where $\text{M}(\text{II})$ is the divalent metal cation and $\text{M}(\text{III})$ is the trivalent metal cation. A^{n-} is the guest anion and “ x ” is the cationic ratio defined as $x = \text{M}(\text{III})/(\text{M}(\text{III}) + \text{M}(\text{II}))$ where $0.20 \leq x \leq 0.40$.^{1,4,5,9–12}

Recently, despite the generally accepted claim¹³ that only ionic radii ranging between 65 and 89 pm for divalent cations and 62 and 69 pm for trivalent cations can form a stable LDH structure, complex hierarchal microspheres of cadmium–aluminum layered double hydroxide ($r_{\text{Cd}} = 109$ pm) were synthesized using a reaction-diffusion framework (RDF) and shown to exhibit interesting photocatalytic activity for the reduction of carbon dioxide.¹⁴

Received: March 22, 2016

Revised: June 15, 2016

Published: June 23, 2016

In this paper, we aim to continue to explore the CdAlA LDH and hereby present a study of the intercalation of a fluorescent dye, rhodamine B (RhB), during the formation of the CdAlA LDH and the de-intercalation of this dye during the transition from the CdAlA LDH into the β -Cd(OH)₂ (Figure 1) using

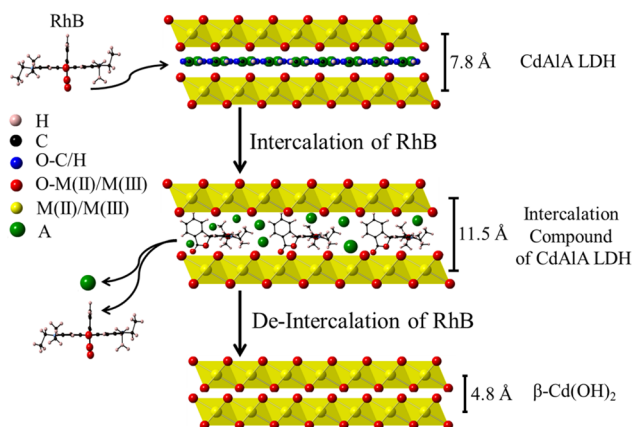


Figure 1. Schematic representation of RhB intercalation between the brucite-like sheets of the CdAlA LDH and its de-intercalation during the polymorphic transformation into the β -Cd(OH)₂.

RDF in combination with *in situ* steady-state and time-resolved fluorescence spectroscopy. O'Hare and co-workers¹⁵ monitored the intercalation of a limited number of hosts in some LDHs (LiAl and CaAl LDHs) using *in situ* energy dispersive X-ray diffraction (EDXRD). This *in situ* method permitted the detection of metastable species, known as staging intermediates, during the intercalation and de-intercalation processes. Accordingly, they were able to examine the kinetics of intercalation using a solid-state reaction model derived by Avrami, where the collected data was fitted with the Avrami–Erofe'ev equation and the activation energies (E_a) were calculated.¹⁵ Also, they were able to detect the phase conversion of some LDH-like compounds (α -Co(OH)₂) to brucite-like compounds (β -Co(OH)₂) using *in situ* small/wide-angle X-ray scattering (SAXS/WAXS).¹⁶ These methods are restricted to slow transformations and are only applicable to a narrow class of LDHs such as LiAl and CaAl LDHs. Thus, for other types of LDHs (such as MgAl LDH and FeAl LDH), where reactions are fast, it is impossible to determine the kinetic parameters.

RDF provides an alternative to the aforementioned technique and allows the calculation of the kinetic parameters of intercalation/de-intercalation of RhB, for a range of LDH/brucite compounds.

RhB (Figure S1A,B) is a xanthene derivative emitting in the red (550–640 nm) region of the visible spectrum. RhB is a cationic probe in acidic medium and a neutral one in basic solution.¹⁷ We will see that one advantage of RDF lies in the ability to intercalate, with ease, neutral molecules such as RhB inside layered and porous materials. The excitation and emission spectra, in addition to the lifetime values of RhB, are sensitive to the changes in the molecular environment of the dye,^{18–20} providing useful information about the conformation and dynamics of the dye itself in the corresponding medium.²¹

THE REACTION-DIFFUSION FRAMEWORK

In our group, we work within a reaction-diffusion framework (RDF) where an outer electrolyte solution is poured on top of an agar gel matrix containing the inner electrolytes. The concentrations of the inner and outer electrolytes are chosen so that a supersaturation gradient is established through the reactor (a tube in this work). This supersaturation gradient furnishes a propagating front leading to the growth of the solid product in its wake. The gel plays a major role in the method for many reasons. First, it provides solid support for the reaction mixture allowing the reactants to diffuse without any convective forces or sedimentation. Second, it slows down the nucleation and growth processes allowing the product extraction at any time. Finally, it provides a suitable platform to perform with ease *in situ* analysis of the reaction zone. Recently, the cosynthesis of β -Co(OH)₂ and α -Co(OH)₂ was also reported using RDF.²² RDF allowed the study of the kinetics of inter and de-intercalation of anions during the formation of the LDH-like, α -Co(OH)₂, and its polymorphic transformation into the β phase, β -Co(OH)₂, via fluorescence spectroscopy.²³ The intercalation and de-intercalation activation energies of anions were calculated and showed that the polymorphic transition was accompanied by an Ostwald ripening mechanism.²³

EXPERIMENTAL SECTION

Materials. All the chemicals were used without any further purification. Rhodamine B, cadmium chloride, cadmium nitrate, aluminum chloride, aluminum nitrate, and sodium hydroxide pellets were supplied by Sigma-Aldrich. Agar gel was purchased from Invitrogen.

Preparation Method. We prepare stock solutions, using double distilled water, of the desired salts mixtures (e.g., aluminum chloride and cadmium chloride) with cationic ratio “ x .” We then add a certain amount (1% w/w) of agar gel weighed using an analytical balance. Next, we heat and stir the mixture until total dissolution of the gel, and we transfer the gel-salts solution into a test tube. We leave the mixture (inner electrolyte) for 2 h to polymerize, at constant ambient temperature. After complete gelation, 1 M sodium hydroxide (outer electrolyte) is poured into the tube provoking the initiation of the reaction-diffusion process. The tube is left for 2 days to allow the formation of both polymorphs, CdAlA LDH and β -Cd(OH)₂ (Figure 2). The extraction of the solids consists of separating the white (β -Cd(OH)₂) and yellow (CdAlA LDH) bands and washing them apart in two different beakers containing double-distilled water and under continuous heating (~ 80 °C) to redissolve the agar gel. We then separate the solid from the solution by centrifugation of the mixture.

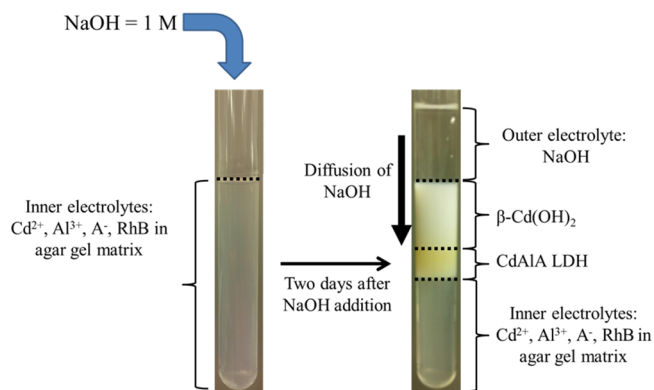


Figure 2. Schematic representation of the coprecipitation of the β -Cd(OH)₂ brucite-like crystals and the CdAlA LDH.

Finally, we freeze-dry the extracted solid for 12 h, and we recollect it for analysis.

Polymorphs Characterization. X-ray powder diffraction (XRD) patterns were carried out by a Bruker D8 Advance XRD diffractometer using Cu-K α radiation ($\lambda = 0.15406$ nm) at 40 kV and 40 mA, ranging from 5° to 50° at a scanning rate of 2°/min and a step size of 0.01 s. Detector scan, rocking curve, and Z-alignment were performed to achieve a better focusing of the X-ray beam. The powder samples were supported on a silver holder via glass slides, and the analysis time was 6 h for all samples. Fourier transform infrared (FT-IR) spectra were recorded on a Thermo Nicolet 4700 Fourier transform infrared spectrometer equipped with a class 1 laser. Powdered samples were mixed with KBr (containing 5 wt % sample) and then a disk-shaped pellet was formed. The thermal behavior of the precipitates was studied using thermal gravimetric analysis (TGA) on a TG 209 F1 Iris (Netzsch, Germany), in nitrogen atmosphere and a temperature range from 40 to 500 °C, with a heating rate of 10 °C/min. The thermal decomposition of the products was also studied using a differential scanning calorimeter (DSC 204 F1 Phoenix, Netzsch, Germany). The heating rate was 10 °C/min under a nitrogen atmosphere with a flow rate of 40 mL/min. ^{13}C Solid-state nuclear magnetic resonance (SSNMR) experiments were conducted using a Bruker 400 MHz SS-NMR AVANCE III spectrometer (Bruker Bio Spin, Rheinstetten, Germany). All samples were prepared by packing 50 mg of the samples in standard 4 mm zirconia rotors from Bruker and sealed at the open end with a Vespel cap. ^{13}C Cross-polarization magic angle spinning (CP MAS) NMR spectra were recorded at a resonance frequency of 100.622 MHz under 12 kHz spinning rate. To achieve a high signal-to-noise ratio, the spectra were recorded by collecting 6 k scans with a recycle delay time of 7 s. The cross-polarization (CP) contact time was set to 2 ms employing ramp 100 for variable amplitude CP. The ^{27}Al SSNMR spectra were recorded by collecting 1024 transients with 2 s recycle delay at 14 kHz spinning rates using WB AVANCE III 400 MHz SS NMR spectrometer equipped with a Double Resonance Broadband BB/1H 4 mm Bruker CP/MAS probe. The duration of excitation pulse was set to 2 μs at an excitation power level of 56.3 W, and the spectral width was set to 480 ppm. Prior to Al acquisition, the Al chemical shift was optimized using aluminum hydroxide as external reference. The EDX characterization of iridium-coated samples was performed on EDX from Ametek with a retractable EDAX detector model Appolo XL mounted on Quanta 600 FEG from FEI running at 2.0 kV. The fluorescence micrographs were taken using a Nikon Eclipse Ti. All the photographs were taken by a Nikon DS-Fi1C camera and under same conditions of light power and intensity. The steady-state fluorescence measurements were recorded using a Varian fluorescence spectrophotometer (Cary Eclipse), where the excitation and emission slits were 5 and 2.5 nm respectively, and the photomultiplier tube (PMT) voltage was 700 V. All the fluorescence measurements were performed in a 5 mL fluorescence cuvette containing the inner electrolytes in gel medium together with 0.1 μM of RhB as a fluorescent probe. The excitation and emission spectra were carried out in front face geometry by focusing the beam on the LDH formation front to detect the intercalation and on the LDH/brucite interface to detect the de-intercalation of the RhB molecules. The temperature was controlled by connecting an external thermostat to the sample holder. Time resolved fluorescence spectra were recorded using a Jobin-Yvon-Horiba Fluorolog III fluorometer operating at 800 V. The powder sample was excited with a 458 nm pulsed light. The detection rate (α) was 1 photon for each 100 excitation pulses and the peak preset was 25 000 counts. Finally, Data Analysis Software was used for decay fitting.

RESULTS AND DISCUSSION

The extracted precipitates (yellow (CdAlA LDH) and white (β -Cd(OH) $_2$) are characterized using a range of spectroscopic techniques. Fluorescence microscopy, XRD, and SSNMR are applied to investigate the presence of RhB. Finally, the kinetics of intercalation and de-intercalation are examined using steady-state and time-resolved fluorescence spectroscopy.

Chemical Composition. The stoichiometry of each LDH is determined based on the analysis of the TGA curves (Figure S2) and the EDX data (Figure S3). Therefore, the amount of water (adsorbed and intercalated) is determined from the TGA measurements;²⁴ the cationic ratio “ x ” of the LDHs and the quantity of intercalated anions (chlorides and nitrates) are calculated from the atomic percentages given by the EDX spectra. Finally, the exact amount of carbonates is calculated from the TGA data.²⁴ The obtained empirical formulas for different CdAlA LDHs are given in Table 1.

Table 1. Empirical Formulas of Different CdAlA LDHs

$x = 0.25$	
A = Cl $^-$	[Cd $_{0.75}$ Al $_{0.25}$ (OH) $_2$](Cl) $_{0.19}$ (CO $_3$) $_{0.03}$ ·0.4H $_2$ O
A = NO $_3^-$	[Cd $_{0.75}$ Al $_{0.25}$ (OH) $_2$](NO $_3$) $_{0.17}$ (CO $_3$) $_{0.04}$ ·0.39H $_2$ O
$x = 0.33$	
A = Cl $^-$	[Cd $_{0.67}$ Al $_{0.33}$ (OH) $_2$](Cl) $_{0.25}$ (CO $_3$) $_{0.04}$ ·0.4H $_2$ O
A = NO $_3^-$	[Cd $_{0.67}$ Al $_{0.33}$ (OH) $_2$](NO $_3$) $_{0.27}$ (CO $_3$) $_{0.03}$ ·0.41H $_2$ O

The chemical composition of the β phase is also determined from the atomic composition data given by the EDX spectrum (Figure S4). The chemical formula of the β phase resulting from the polymorphic transformation of all CdAlA LDHs is Cd(OH) $_2$, where the atomic ratio O/Cd varies between 1.9 and 2.05. The absence of the aluminum hydroxide Al(OH) $_3$ phase is due to its dissolution in excess diffusing hydroxide ions.

X-ray Diffraction. XRD is a useful technique for the characterization of LDHs, and it allows the identification of different polymorphs.²³ LDHs share a similar characteristic diffraction pattern with two main peaks at 2θ values around 11° and 23°. Figure 3B,C shows the diffraction patterns of

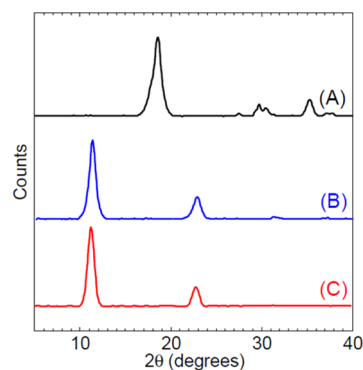


Figure 3. XRD patterns of the white polymorph (β -Cd(OH) $_2$) (A) and the yellow polymorph (CdAlA LDH) for $x = 0.25$ (B) and $x = 0.33$ (C).

different CdAlA LDHs (for $x = 0.25$ and $x = 0.33$). The two main Bragg reflection peaks are observed at 11.3° and 22.6°, which are indexed as the (003) and (006) reflections, respectively. Thus, using Bragg's equation ($n\lambda = 2d \sin \theta$) and the equation relating the “ d ” spacing to the (hkl) indices for a rhombohedral unit cell, the lattice parameter c ($c = 3d(003)$) is calculated.

Figure 3A presents the diffraction patterns of the white polymorph. All the diffraction peaks can be indexed to β -Cd(OH) $_2$ in a hexagonal symmetry.²⁶ Table 2 presents the values of the lattice parameter “ c ” for both polymorphs.

Differential Scanning Calorimetry. DSC is a common technique used for the thermal analysis of LDHs.^{27,28} In

Table 2. Unit Cell Parameter “*c*” of the β -Cd(OH)₂ Crystals and CdAlA LDHs Having Different Cationic Ratios and Interlayer Anions

	CdAlCl LDH (Å)	CdAlNO ₃ LDH (Å)	β -Cd(OH) ₂ (Å)
<i>x</i> = 0.25	23.68	23.68	4.77
<i>x</i> = 0.33	23.27	23.27	4.77

general, DSC measurements show two endothermic peaks.²⁸ The first peak occurs at a relatively low temperature and corresponds to the loss of adsorbed and interlayer water. The second peak occurs at higher temperatures; it may consist of two stages, and it is due to dehydroxylation of the brucite sheets.

In Figure 4B,C, all the CdAlA LDHs show a main heat flow step between 70 and 148 °C corresponding to the loss of adsorbed and interlayer water.

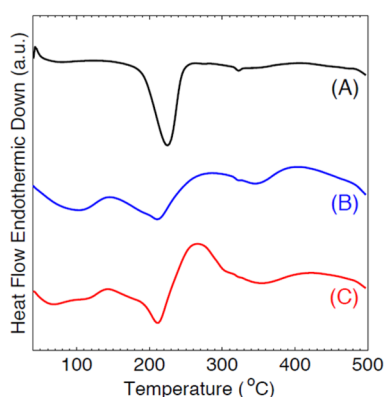


Figure 4. DSC plots of the β -Cd(OH)₂ crystals (A), CdAlA LDH for *x* = 0.25 (B) and *x* = 0.33 (C).

The heat flow at 210 °C is attributed to Cd–OH dehydroxylation, while the peak at 350 °C is due to Al–OH dehydroxylation together with the loss of interlayer anions.^{24,29} The shoulder at 300 °C is attributed to the decarbonation.²⁴ In contrast, the DSC spectrum of β -Cd(OH)₂ (Figure 4A) shows only one endothermic peak at 210 °C attributed to Cd–OH dehydroxylation.

FT-IR Spectroscopy. FT-IR spectroscopy is used to examine the presence of guests anions based on their vibrational modes.²⁷ Figure 5A,B shows the FT-IR spectra of CdAlA LDHs with different guest anions. The broad peak at 3450 cm⁻¹, present in both LDHs, is assigned to the OH stretching vibration of the interlayer and surface bound water. The shoulder at 2950 cm⁻¹ is attributed to the hydrogen bonding between water and anions in the interlayer region.²⁷ The water bending vibration also gives a peak at 1635 cm⁻¹. The carbonate anions present three peaks at around 1350 cm⁻¹, 875 and 625 cm⁻¹ that are attributed to the antisymmetrical stretching mode ν_3 (*E'*), the out-of-plane bending mode ν_2 (*A₂'*) and the bending angular mode ν_4 (*E'*), respectively. The symmetric stretching mode ν_1 (*A₁'*) is infrared inactive. The peak at 1355 cm⁻¹ (Figure 5B) is assigned to the ν_3 antisymmetric stretching vibration of the N–O bond. The peak in the low wavenumber region at 460 cm⁻¹, typical for the brucite structure (Figure 5C), is due to the vibration of Cd–O. The sharp peak at 3610 cm⁻¹ (Figure 5C) is attributed to the O–H stretching mode of the free Cd–OH in the β -Cd(OH)₂. This peak is absent in the CdAlA LDHs because the free Cd–

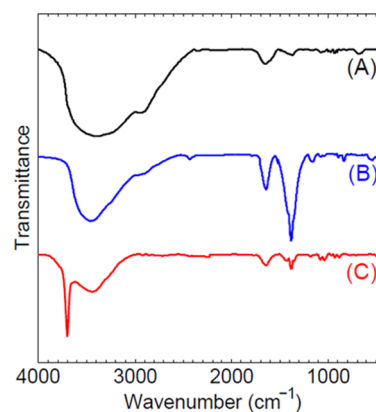


Figure 5. FT-IR spectra of the CdAlA LDH intercalated with chloride (A) and nitrate (B) anions and that of the brucite-like β -Cd(OH)₂ crystals (C).

OH in the positively charged layers is interacting with the interlayer anions through hydrogen bonding.²³

²⁷Al Solid-State NMR. ²⁷Al SSNMR spectroscopy is used to investigate the aluminum coordination of the CdAlA LDHs. The chemical shift of the NMR signals of ²⁷Al can be used to differentiate between the octahedral (Al_(octa)) and the tetrahedral (Al_(tetra)) coordinations, where the range of the chemical shift of Al_(tetra) is 110 ppm–90 ppm while that of Al_(octa) is 20 ppm–0 ppm.³⁰ All the prepared CdAlA LDHs exhibit a peak at a chemical shift around 15 ppm (Figure S5), providing evidence for the octahedral coordination. This slight shift from the perfectly octahedral environment ($\delta = 0$ ppm) is due to minor changes in the O–Al bond length.³¹

Kinetics of RhB Intercalation in Different CdAlA LDHs.

The excitation and emission fluorescence spectra of RhB in the presence of different Cd²⁺/Al³⁺ mixtures in the agar matrix display a blue shift of 3–4 nm (excitation ~559 nm and emission ~579 nm) compared to those in water (excitation ~562 nm and emission ~583 nm). This shift is due to the change in the chemical environment of the probe inside the agar gel matrix compared to that in the water solution.^{20,32}

Also, the measured solid-state fluorescence lifetime of RhB in all the prepared CdAlA LDHs exhibit two time components of 1.4 ns (32%) and 5.1 ns (68%). The shorter time component (1.4 ns) is attributed to the RhB adsorbed on the LDH surface which is relatively close to that of RhB in gel or water (1.6 ns). Solid-state fluorescence lifetime measurements are performed on both Cd(OH)₂ and Al(OH)₃ prepared in the presence of RhB using RDF. One time component of 1.4 ns is obtained. On the other hand, the longer time component (5.1 ns) is attributed to the intercalated RhB molecules. The increase in the fluorescence lifetime upon intercalation is quantified using the Forster–Hoffman equation given by

$$\tau = C_m \eta^\alpha$$

where “ τ ” is the probe’s lifetime, “ C_m ” is a constant depending on the medium’s temperature and fluorophores’ concentration, “ α ” is the probe dependent molecular parameter, and “ η ” is the medium’s viscosity. According to some findings in the literature,^{33,34} a category of xanthene dyes shows a lifetime dependence on the degree of motion of the organic substituents of the amine group if existed.^{33,34} The degree of motion of the –NR₁R₂ group plays a significant role in determining the rate of internal conversion. In our work, the

increase in the probe's (RhB) lifetime can be attributed to the restriction of the mobility of $-NR_1R_2$ ($R_1 = R_2 = C_2H_5$) upon intercalation.³⁵

This phenomenon was explained by Drexhage,³⁵ who studied the lifetime dependence of the xanthene dyes on the amino group's flexibility. Thus, upon excitation and due to the rotation ability along the C–N bonds, these dyes show a distortion in their excited state to form a twisted intramolecular charge transfer state (TICT).^{36–38} This charge transfer results in a nonradiative decay leading to smaller values of the fluorescence lifetime.³³

The intercalation of RhB is further examined via fluorescence microscopy, ¹³C SSNMR XRD and ²⁷Al SSNMR. The fluorescence image of the extracted CdAlA LDH (Figure 6) after washing out the gel presents significant fluorescence of CdAlA LDH, indicating that the RhB probes are adsorbed and/or intercalated.

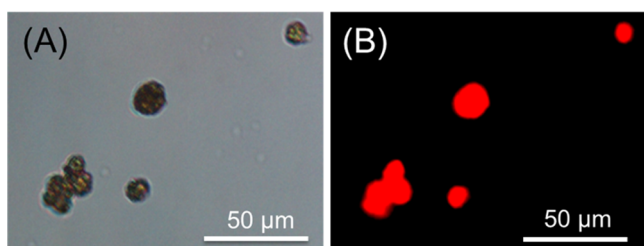


Figure 6. Microscopic image of CdAlA LDH particles intercalated with RhB; under visible light (A) and fluorescence microscopic image of the same particles (B).

Furthermore, the ¹³C SSNMR spectrum in Figure S6 shows several aromatic peaks ranging between 105 and 130 ppm as well as several aliphatic peaks in the range between 5 and 40 ppm, which gives further indication that the RhB molecules are adsorbed and/or intercalated between the brucite-like sheets of the CdAlA LDH.

Moreover, the XRD patterns of the extracted CdAlA LDHs prepared in the presence of RhB reveal a new reflection at 7.7° for different CdAlA LDHs (Figure 7A). This reflection corresponds to the shift of the (003) peak due to the intercalation of the dye. Table 3 shows the calculated lattice parameter “c” for different CdAlA LDHs prepared in the presence of RhB. Consequently, the increase in the interlayer

Table 3. Unit Cell Parameter “c” of Different CdAlA LDHs Intercalated with RhB Probes

	CdAlCl LDH (Å)	CdAlNO ₃ LDH (Å)
$x = 0.25$	34.42	34.42
$x = 0.33$	34.42	34.42

spacing value from 23.5 Å (absence of RhB) to 34.5 Å (presence of RhB) indicates that the RhB molecules are incorporated into the interlayer region. This shift corresponds to an increase in the interlayer spacing from 3.0 to 6.7 Å, which matches the side dimension of RhB (Figure S1B). Therefore, the most probable arrangement of RhB between the LDH's layers (Figure 7B), assuming that the intercalation of RhB does not alter the structure of the sheets, is parallel to the brucite-like sheets as shown in Figure 7C.

Furthermore, upon formation of the different CdAlA LDHs in the gel and in the presence of RhB, the fluorescence intensity decreases in a first exponential decay. The excitation and emission maxima are 554 and 572 nm, respectively; thus, the incorporation of RhB between the LDH's sheets resulted in a blue shift of these maxima compared to those in the agar matrix. Figure S7 shows the fluorescence spectra (excitation and emission) of RhB during the formation of CdAlA LDH. The observed blue shift is due to the interaction between the RhB's xanthene rings and the positive charges of the brucite-like sheets which is examined via ²⁷Al SSNMR (Figure S8). The ²⁷Al SSNMR spectrum of CdAlA LDH intercalated with RhB shows two distinct peaks at $\delta = 15$ ppm and $\delta = 75$ ppm, while the non-intercalated CdAlA LDH presents only one peak at $\delta = 15$ ppm. This splitting suggests the interaction of the LDH's sheets with the intercalated RhB molecules leading to a different chemical environment around the aluminum atoms.³¹

The rate constants “k” of RhB intercalation inside the interlayer region of CdAlA LDHs having different cationic ratios and interlayer anions are calculated by fitting the plots of the variation of the fluorescence signal measured at $\lambda_{em}(\max) = 573$ nm versus time which presents a first exponential fluorescence decay (Figure 8).

Consequently, the activation energies of RhB intercalation in different CdAlA LDHs are calculated from the Arrhenius equation given by

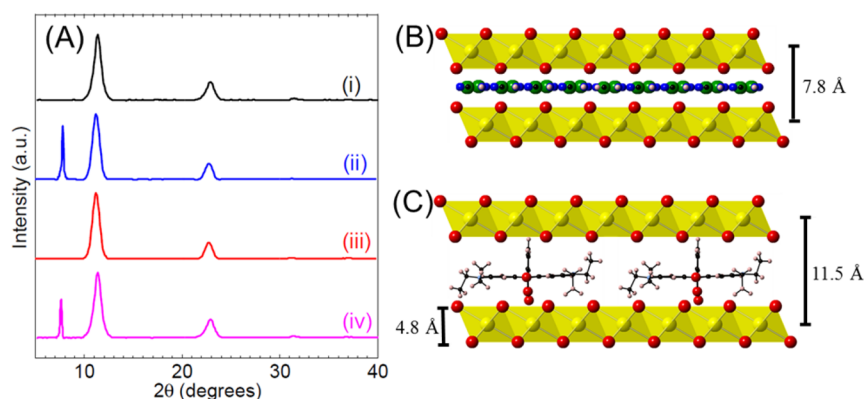


Figure 7. (A) XRD spectra of CdAlA LDH ($x = 0.25$) (A(i)), CdAlA LDH ($x = 0.25$) intercalated with RhB (A(ii)), CdAlA LDH ($x = 0.33$) (A(iii)), and CdAlA LDH ($x = 0.33$) intercalated with RhB (A(iv)). CdAlA brucite-like sheets (B) and probable arrangement of RhB intercalated between the brucite-like sheets (C).

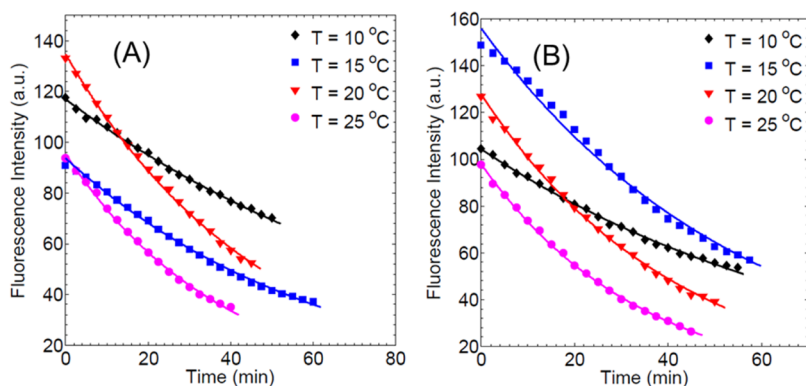


Figure 8. Kinetic plots of the fluorescence intensity of RhB during its intercalation in CdAlNO₃ LDH having a cationic ratio of $x = 0.25$ (A) and $x = 0.33$ (B). All fits are reported with correlation coefficient (r^2) higher than 0.992.

$$\ln k = \ln A - \left(\frac{E_a}{R}\right) \frac{1}{T}$$

where “ k ” is the rate constant of RhB molecules’ intercalation at a given temperature “ T ”, and “ E_a ” is the corresponding activation energy. Table 4 shows the activation energies of

Table 4. Activation Energies of RhB’s Intercalation in Different CdAlA LDHs

	CdAlCl LDH (kJ mol ⁻¹)	CdAlNO ₃ LDH (kJ mol ⁻¹)
$x = 0.25$	39.2 ± 0.5	39.0 ± 0.6
$x = 0.33$	41.6 ± 0.4	41.7 ± 0.6

RhB intercalation in different CdAlA LDHs. Figure S9 shows the Arrhenius plots used to calculate the activation energies of RhB intercalation in CdAlNO₃ LDHs for two different “ x ” values.

Kinetics of RhB De-Intercalation during the Transition into the β -Cd(OH)₂. During the polymorphic transformation of CdAlA LDH into β -Cd(OH)₂, the fluorescence intensity increases continuously (Figure S10) until it reaches a plateau at the end of the transition. The excitation and emission maxima of RhB are recorded to be 559 and 579 nm, respectively. These maxima are red-shifted by ~6 nm compared to those of RhB intercalated in the LDH and are equal to those of RhB in the agar gel matrix. This red shift throughout the transition into β -Cd(OH)₂ can be assigned to the release of RhB from the interlayer region of the LDH.

On the other hand, the extracted β -Cd(OH)₂ crystals show a weak fluorescence (Figure 9).

Also, the ¹³C SSNMR spectrum of β -Cd(OH)₂ solid (Figure S11) did not exhibit a carbon signal. Both results suggest either

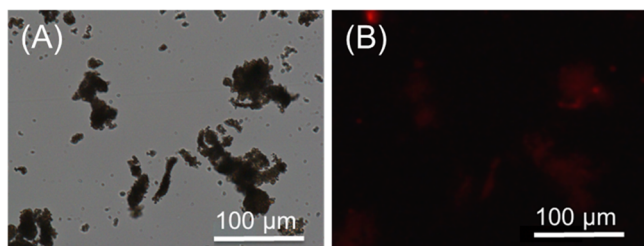


Figure 9. Microscopic image of β -Cd(OH)₂ prepared in the presence of RhB; under visible light (A) and fluorescence microscopic image of the same particles (B).

the absence of RhB or the presence of undetectable adsorbed traces. The solid-state fluorescence lifetime presents a one time component of 1.4 ns, which corresponds to the adsorbed RhB on the surface of β -Cd(OH)₂.

Moreover, identical XRD patterns are obtained for the β -Cd(OH)₂ crystals prepared in the presence and absence of RhB (Figure S12). Therefore, all these techniques indicate that while some RhB molecules remain adsorbed on the brucite surface, the brucite compound (β -Cd(OH)₂) cannot accommodate RhB molecules in its small cavities.

Similar to the intercalation kinetics, the different rate constants of RhB de-intercalation during the transition from the CdAlA LDH to β -Cd(OH)₂ are calculated by fitting the plots of the fluorescence intensity variation with time (Figure 10). The monoexponential fit of the fluorescence suggests that the change of intensity corresponds to the de-intercalation of the used probe. Moreover, the corresponding activation energies are determined from the Arrhenius plots (Figure S13), as previously described. Table 5 summarizes the calculated activation energies of RhB de-intercalation during the conversion of different CdAlA LDHs to β -Cd(OH)₂.

Proposed Mechanism. Fluorescence resonance energy transfer (FRET) is a long-range dipole–dipole interaction between the excited electronic state of a donor molecule and the ground state of an acceptor one. The rate of energy transfer depends on several factors, mainly the distance between the donor and acceptor (~5 nm), the extent of spectral overlap between the acceptor’s absorption and donor’s emission spectra, and the donor’s quantum yield.³⁹ There are two types of RET: the homo-RET where the donor–acceptor probes are chemically identical and the hetero-RET where they are chemically distinct.⁴⁰ The homo-RET occurs for fluorescent dyes exhibiting small Stokes shift. RhB presents a Stokes shift of 17 nm. Besides, the possibility of the homo-RET for a given fluorescent dye is assessed by examination of the overlap’s extent between absorption and emission spectra. Figure S14 indicates that the homo-RET event can occur in the case of RhB due to the considerable spectral overlap extent between its absorption and emission spectra.

Furthermore, in the gel medium, the fluorophores are too far apart due to the low concentration of RhB (100 nM); consequently, the homo-RET event is unlikely to occur. Moreover, none of the salts present in the medium show any quenching effect on the fluorescence signal of the involved probe (Table 6). Besides, upon formation of the CdAlA LDH, the RhB molecules are intercalated in the interlayer region of

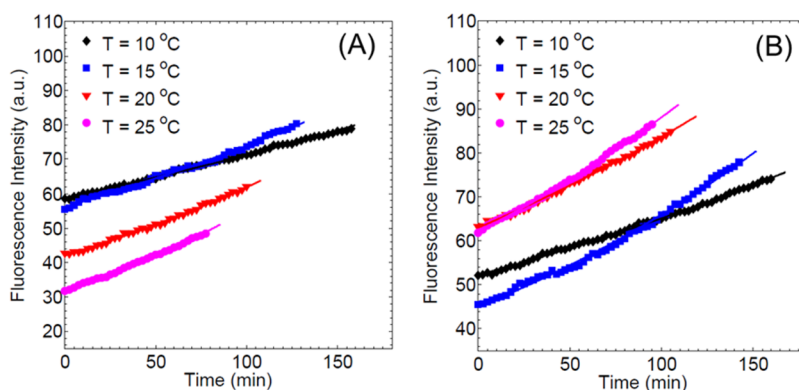


Figure 10. Kinetic plots of the fluorescence intensity of RhB during its de-intercalation from the CdAlNO₃ LDH having a cationic ratio of $x = 0.25$ (A) and $x = 0.33$ (B). All fits are reported with correlation coefficient (r^2) higher than 0.992.

Table 5. Activation Energies of RhB's De-Intercalation from Different CdAlA LDHs upon Transition into the β -Cd(OH)₂ Crystals

	CdAlCl LDH/ β -Cd(OH) ₂ (kJ mol ⁻¹)	CdAlNO ₃ LDH/ β -Cd(OH) ₂ (kJ mol ⁻¹)
$x = 0.25$	48.5 ± 0.3	48.4 ± 0.9
$x = 0.33$	48.7 ± 0.5	48.8 ± 0.5

the LDH resulting in a local increase in their concentration.⁴¹ Consequently, the average distance between the RhB molecules decreases, which leads to the quenching of the fluorescence signal via homo-RET.

On the other hand, the activation energies of RhB intercalation (Table 4) show a difference of approximately 2.5 kJ mol⁻¹ for CdAlA LDHs having different cationic ratios, where $E_a = 39.1$ kJ mol⁻¹ for $x = 0.25$ and 41.6 kJ mol⁻¹ for $x = 0.33$.^{27,42} Besides, the basal spacing of LDHs is inversely proportional to its cationic ratio, which is previously verified by the XRD data. Accordingly, the RhB molecules require more energy to intercalate as the basal spacing decreases, which clarifies the 2.5 kJ mol⁻¹ difference in the activation energies for different “ x ” values. Besides, a slight difference in the activation energies is observed for the CdAlA LDHs having different interlayer anions (Cl⁻ or NO₃⁻). Hence, the intercalation of RhB in the cavities of LDHs shows a dependence on the cationic ratio of the corresponding LDH and an independence of the interlayer anions nature.

The de-intercalation of RhB during the transition from the CdAlA LDHs, with different intergallery anions and cationic ratios, into the β phase, shows a slight difference in the activation energies which are almost equal to 48.5 kJ mol⁻¹. Yet, the difference in the activation energies between intercalation and de-intercalation is ~ 7 kJ mol⁻¹ when $x = 0.33$ and ~ 9.4 kJ mol⁻¹ when $x = 0.25$. This disparity suggests that the stabilization effect of the RhB probes depends on the interlayer spacing between the brucite sheets. Therefore, the further excess in the positive charges as “ x ” becomes larger causes the destabilization of the probes inside the cavities, and consequently, less energy is needed to break these interactions.

Table 6. Fluorescence Intensity of RhB Prepared in the Presence of Different Salts

mixture ($V_{\text{total}} = 3$ mL)	distilled water	0.1 M CdCl ₂	0.1 M Cd(NO ₃) ₂	0.1 M AlCl ₃	0.1 M Al(NO ₃) ₃	1 M NaOH
fluorescence intensity	180	178	183	184	179	180

CONCLUSIONS

We used the reaction-diffusion framework (RDF) combined with *in situ* fluorescence spectroscopy to study the intercalation and de-intercalation kinetics of a neutral fluorescent probe (RhB) between the layers of CdAlA LDH as it formed and later converted to the brucite-like Cd(OH)₂. Concurrently, the cosynthesis and full characterization of the unstable CdAlA LDH and the brucite-like Cd(OH)₂ were performed and reported. We were able to determine both the activation energies of intercalation and the de-intercalation of RhB. SSNMR and XRD were used in order to understand the mechanism of intercalation and the stabilization of the dye in the interlayer of the LDH. The fluorescence experiments were used to determine the activation energies of intercalation and de-intercalation of RhB and clearly demonstrated their dependence on the cationic ratio of the corresponding LDH. Moreover, the energies of de-intercalation were steadily higher than those of intercalation indicating, with the aid of SSNMR experiments, that the dyes were stabilized as a result of the probe–brucite sheets interactions.

ASSOCIATED CONTENT

Supporting Information

The Supporting Information is available free of charge on the ACS Publications website at DOI: 10.1021/acs.cgd.6b00455.

Characterization of the CdAlA LDH and the β -Cd(OH)₂ crystals. The structural and spectral properties of RhB and the proof of its de-intercalation from the brucite crystals (PDF)

AUTHOR INFORMATION

Corresponding Author

*E-mail: mazen.ghoul@aub.edu.lb. Phone: +961 (1)350000. Fax: +961 (1)365217.

Notes

The authors declare no competing financial interest.

ACKNOWLEDGMENTS

D.S. and M.G. gratefully acknowledge the funding provided by the American University of Beirut Research Board and by the Lebanese National Council for Scientific Research (LCNSR).

REFERENCES

- (1) Xu, Z. P.; Zhang, J.; Adebajo, M. O.; Zhang, H.; Zhou, C. Catalytic applications of layered double hydroxides and derivatives. *Appl. Clay Sci.* **2011**, *53*, 139–150.
- (2) Liu, Z.; Ma, R.; Osada, M.; Iyi, N.; Ebina, Y.; Takada, K.; Sasaki, T. Synthesis, anion exchange, and delamination of Co-Al layered double hydroxide: assembly of the exfoliated nanosheet/polyanion composite films and magneto-optical studies. *J. Am. Chem. Soc.* **2006**, *128*, 4872–4880.
- (3) Tian, G.-L.; Zhao, M.-Q.; Zhang, B.; Zhang, Q.; Zhang, W.; Huang, J.-Q.; Chen, T.-C.; Qian, W.-Z.; Su, D. S.; Wei, F. Monodisperse embedded nanoparticles derived from an atomic metal-dispersed precursor of layered double hydroxide for architected carbon nanotube formation. *J. Mater. Chem. A* **2014**, *2*, 1686–1696.
- (4) Wang, Q.; O'Hare, D. Recent advances in the synthesis and application of layered double hydroxide (LDH) nanosheets. *Chem. Rev. (Washington, DC, U. S.)* **2012**, *112*, 4124–4155.
- (5) Hu, G.; Wang, N.; O'Hare, D.; Davis, J. Synthesis of magnesium aluminium layered double hydroxides in reverse microemulsions. *J. Mater. Chem.* **2007**, *17*, 2257–2266.
- (6) Plank, J.; Zou, N.; Zhao, Z.; Dekany, I. Preparation and Properties of a Graphene Oxide Intercalation Compound Utilizing Hydrocalumite Layered Double Hydroxide as Host Structure. *Z. Anorg. Allg. Chem.* **2014**, *640*, 1413–1419.
- (7) Wu, X.-L.; Wang, L.; Chen, C.-L.; Xu, A.-W.; Wang, X.-K. Water-dispersible magnetite-graphene-LDH composites for efficient arsenate removal. *J. Mater. Chem.* **2011**, *21*, 17353–17359.
- (8) Wang, Y.; Peng, W.; Liu, L.; Tang, M.; Gao, F.; Li, M. Enhanced conductivity of a glassy carbon electrode modified with a graphene-doped film of layered double hydroxides for selectively sensing of dopamine. *Microchim. Acta* **2011**, *174*, 41–46.
- (9) Zhao, Y.; Li, F.; Zhang, R.; Evans, D. G.; Duan, X. Preparation of layered double-hydroxide nanomaterials with a uniform crystallite size using a new method involving separate nucleation and aging steps. *Chem. Mater.* **2002**, *14*, 4286–4291.
- (10) Liang, H.; Meng, F.; Cabán-Acevedo, M.; Li, L.; Forticaux, A.; Xiu, L.; Wang, Z.; Jin, S. Hydrothermal Continuous Flow Synthesis and Exfoliation of NiCo Layered Double Hydroxide Nanosheets for Enhanced Oxygen Evolution Catalysis. *Nano Lett.* **2015**, *15*, 1421–1427.
- (11) Xu, J.; Gai, S.; He, F.; Niu, N.; Gao, P.; Chen, Y.; Yang, P. A sandwich-type three-dimensional layered double hydroxide nanosheet array/graphene composite: fabrication and high supercapacitor performance. *J. Mater. Chem. A* **2014**, *2*, 1022–1031.
- (12) Wang, B.; Williams, G. R.; Chang, Z.; Jiang, M.; Liu, J.; Lei, X.; Sun, X. Hierarchical NiAl Layered Double Hydroxide/Multiwalled Carbon Nanotube/Nickel Foam Electrodes with Excellent Pseudocapacitive Properties. *ACS Appl. Mater. Interfaces* **2014**, *6*, 16304–16311.
- (13) Goh, K.-H.; Lim, T.-T.; Dong, Z. Application of layered double hydroxides for removal of oxyanions: a review. *Water Res.* **2008**, *42*, 1343–1368.
- (14) Saliba, D.; Ezzeddine, A.; Sougrat, R.; Khashab, N. M.; Hmadeh, M.; Al-Ghoul, M. Cadmium–Aluminum Layered Double Hydroxide Microspheres for Photocatalytic CO₂ Reduction. *ChemSusChem* **2016**, *9*, 800–805.
- (15) Williams, G. R.; O'Hare, D. Towards understanding, control and application of layered double hydroxide chemistry. *J. Mater. Chem.* **2006**, *16*, 3065–3074.
- (16) Du, Y.; Ok, K. M.; O'Hare, D. A kinetic study of the phase conversion of layered cobalt hydroxides. *J. Mater. Chem.* **2008**, *18*, 4450–4459.
- (17) Korobov, V.; Chibisov, A. Primary processes in the photochemistry of rhodamine dyes. *J. Photochem.* **1978**, *9*, 411–424.
- (18) Vitha, M. F.; Clarke, R. J. Comparison of excitation and emission ratiometric fluorescence methods for quantifying the membrane dipole potential. *Biochim. Biophys. Acta, Biomembr.* **2007**, *1768*, 107–114.
- (19) Osborne, A. D.; Winkworth, A. C. Viscosity-dependent internal conversion in an aryl-substituted rhodamine dye. *Chem. Phys. Lett.* **1982**, *85*, 513–517.
- (20) Fikry, M.; Omar, M.; Ismail, L. Z. Effect of host medium on the fluorescence emission intensity of rhodamine B in liquid and solid phase. *J. Fluoresc.* **2009**, *19*, 741–746.
- (21) Hincley, D. A.; Seybold, P. G.; Borris, D. P. Solvatochromism and thermochromism of rhodamine solutions. *Spectrochim. Acta Mol. Biomol. Spectrosc.* **1986**, *42*, 747–754.
- (22) El-Batlouni, H.; El-Rassy, H.; Al-Ghoul, M. Cosynthesis, coexistence, and self-organization of α - and β -cobalt hydroxide based on diffusion and reaction in organic gels. *J. Phys. Chem. A* **2008**, *112*, 7755–7757.
- (23) Rahbani, J.; Khashab, N. M.; Patra, D.; Al-Ghoul, M. Kinetics and mechanism of ionic intercalation/de-intercalation during the formation of α -cobalt hydroxide and its polymorphic transition to β -cobalt hydroxide: reaction–diffusion framework. *J. Mater. Chem.* **2012**, *22*, 16361–16369.
- (24) Klopoggea, J. T.; Kristófb, J.; Frosta, R. L. In *Thermogravimetric Analysis-Mass Spectrometry (TGA-MS) of Hydrotalcites Containing CO₃²⁻, NO₃⁻, Cl⁻, SO₄²⁻ or ClO₄*, 2001, a Clay Odyssey: Proceedings of the 12th International Clay Conference, Bahía Blanca, Argentina, July 22–28, 2001, 2003; Elsevier: Amsterdam, 2003; p 451.
- (25) Cota, I.; Ramírez, E.; Medina, F.; Layrac, G.; Tichit, D.; Gérardin, C. Influence of the preparation route on the basicity of La-containing mixed oxides obtained from LDH precursors. *J. Mol. Catal. A: Chem.* **2016**, *412*, 101–106.
- (26) Eskizeybek, V.; Demir, O.; Avci, A.; Chhowalla, M. Synthesis and characterization of cadmium hydroxide nanowires by arc discharge method in de-ionized water. *J. Nanopart. Res.* **2011**, *13*, 4673–4680.
- (27) Rives, V. *Layered Double Hydroxides: Present and Future*; Nova Publishers: New York, 2001.
- (28) Hamerski, F.; Corazza, M. L. LDH-catalyzed esterification of lauric acid with glycerol in solvent-free system. *Appl. Catal., A* **2014**, *475*, 242–248.
- (29) Souza, A. D.; Arruda, C. C.; Fernandes, L.; Antunes, M. L.; Kiyohara, P. K.; Salomão, R. Characterization of aluminum hydroxide (Al(OH)₃) for use as a porogenic agent in castable ceramics. *J. Eur. Ceram. Soc.* **2015**, *35*, 803–812.
- (30) Al-Bloushi, M.; Davaasuren, B.; Emwas, A. H.; Rothenberger, A. Synthesis and Characterization of the Quaternary Thioaluminogermanates A (AlS₂)(GeS₂) (A = Na, K). *Z. Anorg. Allg. Chem.* **2015**, *641*, 1352–1356.
- (31) Vichi, F. M.; Alves, O. L. Preparation of Cd/Al layered double hydroxides and their intercalation reactions with phosphonic acids. *J. Mater. Chem.* **1997**, *7*, 1631–1634.
- (32) Reissfeld, R.; Zusman, R.; Cohen, Y.; Eyal, M. The spectroscopic behaviour of rhodamine 6G in polar and non-polar solvents and in thin glass and PMMA films. *Chem. Phys. Lett.* **1988**, *147*, 142–147.
- (33) Magde, D.; Rojas, G. E.; Seybold, P. G. Solvent dependence of the fluorescence lifetimes of xanthene dyes. *Photochem. Photobiol.* **1999**, *70*, 737–744.
- (34) López Arbeloa, T. L.; López Arbeloa, F. L.; Hernández Bartolomé, P. H.; López Arbeloa, I. L. On the mechanism of radiationless deactivation of rhodamines. *Chem. Phys.* **1992**, *160*, 123–130.
- (35) Drexhage, K. What's ahead in laser dyes? *Laser Focus* **1973**, *9*, 35–39.
- (36) Tredwell, C. J.; Osborne, A. D. Viscosity dependent internal conversion in the rhodamine dye, fast acid violet 2R. *J. Chem. Soc., Faraday Trans. 2* **1980**, *76*, 1627–1637.

(37) Adhikary, R.; Barnes, C. A.; Trampel, R. L.; Wallace, S. J.; Kee, T. W.; Petrich, J. W. Photoinduced trans-to-cis isomerization of cyclocurcumin. *J. Phys. Chem. B* **2011**, *115*, 10707–10714.

(38) Pal, P.; Zeng, H.; Durocher, G.; Girard, D.; Li, T.; Gupta, A. K.; Giasson, R.; Blanchard, L.; Gaboury, L.; Balassy, A.; Turmel, C.; Laperrière, A.; Villeneuve, L. Phototoxicity of some bromine-substituted rhodamine dyes: Synthesis, photophysical properties and application as photosensitizers. *Photochem. Photobiol.* **1996**, *63*, 161–168.

(39) Selvin, P. R. Fluorescence resonance energy transfer. *Methods Enzymol.* **1995**, *246*, 300–334.

(40) Tramier, M.; Piolot, T.; Gautier, I.; Mignotte, V.; Coppey, J.; Kemnitz, K.; Durieux, C.; Coppey-Moisan, M. Homo-FRET versus hetero-FRET to probe homodimers in living cells. *Methods Enzymol.* **2003**, *360*, 580–97.

(41) Lee, J. H.; Jung, D.-Y.; Kim, E.; Ahn, T. K. Fluorescein dye intercalated layered double hydroxides for chemically stabilized photoluminescent indicators on inorganic surfaces. *Dalton Trans.* **2014**, *43*, 8543–8548.

(42) Cavani, F.; Trifirò, F.; Vaccari, A. Hydrotalcite-type anionic clays: Preparation, properties and applications. *Catal. Today* **1991**, *11*, 173–301.